

Research Article

DinhHieu Tran*, HongGiang Nguyen, YuRen Wang*, KhacHai Phan, ThiTuyetNga Phu, DuyPhuong Le, and TienThinh Nguyen*

Analysis of artificial intelligence approaches to predict the wall deflection induced by deep excavation

<https://doi.org/10.1515/geo-2022-0503>
received March 20, 2023; accepted May 30, 2023

Abstract: The geological condition of Ho Chi Minh (HCM) City is soft soil and high groundwater and includes two main structural layers such as Pleistocene and Holocene sediments. Therefore, deep excavation of all the high-rise buildings in the city is usually supported by concrete retaining walls such as the diaphragm or bored pile retaining walls. The system limits the excavation wall deflection during the construction process which could pose a potential risk to the construction and neighborhood areas. To estimate wall deformation at a highly accurate and efficient level, this study presents several machine learning models including feed-forward neural network back-propagation (FFNN-BP), long short-term memory (LSTM), bidirectional long short-term memory (Bi-LSTM), and support vector regression (SVR). The database for the experiment was obtained from a high building in HCM City, Vietnam. The database is deployed to implement the proposed algorithms in walk-forward validation

technique. As a result, the Bi-LSTM model reduced prediction errors and improved robustness than the LSTM, FFNN-BP, and SVR models. Bi-LSTM, LSTM, and FFNN-PB could be used for predicting deep excavation wall deflection. In the meantime, not only could the estimated results support safety monitoring and early warning during the construction stages but also could contribute to legal guidelines for the architecture of deep excavations in the city's soft ground.

Keywords: excavation, deformation, retaining wall, machine learning and deep learning prediction

1 Introduction

Ho Chi Minh (HCM) City is a pillar and a motivation for the current economic development of Vietnam. In recent years, government, private, and public enterprises have invested and upgraded the utilities, transportation infrastructure, and buildings around the city. There has been a rapid increase in population and development of apartments for rent; hence, the demand for high-rise buildings with basements continuously develops in the city. In designing and constructing high-rise buildings with basements related to retaining walls, basements, and deep excavations, it is necessary to check the displacement of the retaining walls. If the calculation is not reasonable, it will damage neighboring works and works under construction, affecting related structural functions and the durability of the work itself [1–3].

The basements of high-rise buildings are often supported by permanent concrete retaining walls (PCRWs) [4]. In addition, PCRW is known as one of the most commonly implemented cover methods, particularly for deep excavations on the soft ground [5,6]. Furthermore, PCRW minimizes wall deflection to protect the excavation itself as well as the utilities and structures around construction areas. Hence, it is crucial to estimate wall deformation

* Corresponding author: DinhHieu Tran, Faculty of Architecture, Thu Dau Mot University, ThuDauMot 820000, Vietnam, e-mail: hieutd@tdmu.edu.vn

* Corresponding author: YuRen Wang, Department of Civil Engineering, National Kaohsiung University of Science and Technology, Kaohsiung 80778, Taiwan, e-mail: yrwang@nkust.edu.tw, tel: +8490 515 3333

* Corresponding author: TienThinh Nguyen, Department of International Business, National Kaohsiung University of Science and Technology, Kaohsiung 82445, Taiwan, e-mail: ngtienthinh101096@gmail.com

HongGiang Nguyen: Department of Academic and Students' Affairs, Hue University, Hue City 49000, Vietnam; Department of Civil Engineering, National Kaohsiung University of Science and Technology, Kaohsiung 80778, Taiwan, e-mail: giangnh@hueuni.edu.vn, gianghueuni@gmail.com

KhacHai Phan: Geotech Science Co., Ltd, New Taipei City 22103, Taiwan, e-mail: khachai.ts@gmail.com

ThiTuyetNga Phu: Faculty of Architecture, Thu Dau Mot University, ThuDauMot 820000, Vietnam, e-mail: ngaptt@tdmu.edu.vn

DuyPhuong Le: Department of Planning and Investment of Tay Ninh Province, Tay Ninh, 840000, Vietnam, e-mail: Phuongktsaigon@gmail.com

accurately [7–11]. Several techniques to estimate excavation wall deformation may be divided into numerical simulation and empiric expression. The empirical expression has relied on historical constructions that are relatively easy in model and simple in conducting [12–14]; however, the prediction results often tend to be broad, and the expression cannot stand for the development of wall deflection in progress. On the other hand, the numerical simulation's difficulty is theoretically more specific by examining the soil form behaviors. However, taking all of the basic and vanishing components into account is still difficult, and there is usually a discrepancy between anticipated results and field measurements [4,15].

Due to crucial strict safety requirements in the construction process of the buildings to have basements, researchers and engineers have extensively assessed the lateral wall movement induced by excavations, such as using parametric research using 3D numerical techniques to estimate the wall movement [16,17] or analyzing time-dependent behavior in deep excavation with finite element analysis [18–20].

Deploying the computation technique for geotechnical engineering has quickly advanced recently. Machine learning and deep learning have been used in deep excavations and tunnel excavations such as ground surface settlement and wall deflection [9,21–27]. Zhang et al. [23] used a multivariate adaptive regression splines (MARS) algorithm for examining horizontal wall deflection envelope for braced excavations in clays. The study result indicated that the MARS algorithm is of good interpretability and enables the design engineer to estimate the shape of the wall deflection profiles. Chen et al. [28] used six machine learning algorithms to predict tunnel settlements, namely general regression neural network (GRNN), wavelet neural network, random forest (RF), feed-forward neural network back-propagation (FFNN-BP), extreme machine learning, and support vector machine. The result of the research pointed out that the estimations based on GRNN and RF algorithms are more trustworthy. Goh et al. [29] used FFNN-BP techniques to predict maximum wall deflections induce by braced excavations in soft clay. The highlight method is can be to retraining as obtainable data from finite element experiment and actual field records are obtained. Zhang et al. [30] used Xtreme gradient boosting (XGBoost), RF regression (RFR), decision tree regression (DTR), multilayer perceptron regression (MLPR), and MARS to estimate the maximum lateral wall deformation. The results indicated that XGBoost and RFR outperform DTR, MLPR, and MARS in the dataset of sparse distribution predictions and a stable feature. Deep learning methods are regarded as a subset of the evolution of machine learning. The methods have a deeper structure

and can study much more complicated nonlinear characteristics than traditional neural networks. The study can be supervised, semi-supervised, or unsupervised. There are several successful applications of deep learning in domains. It has attained good outputs for experimental application in the active and deep processing of enormous, long-term, dependent datasets [31,32]. Qu et al. [33] developed the long short-term memory (LSTM) model to estimate concrete dam deformation. The algorithm's outputs showed high estimating accuracy and great robustness, externality, and generalization for the single-point predicted algorithm and multipoint synchronized predicted algorithm for concrete dam deformation. Li et al. [34] proposed an LSTM algorithm to estimate tunnel boring machine (TBM) performances consisting of the sum thrust and the cutter-head torque in an actual time. The research results implied that the experimental approach could acceptably mirror the thrust variation total. The cutter-head torque was better than the classical theoretical approach, offering a single value with a geological strength measurement. Zhao et al. [4] used LSTM to predict diaphragm wall deflection induced by excavation. The result indicated that the LSTM algorithm maintained acceptable performance even in long-term predicting assignments. And the model outperformed BPNN in all prediction locations. Liu et al. [35] used bidirectional LSTM (BiLSTM) and LSTM to predict the working face's ground settlement due to the vibration of TBM. The research results indicated that based on the proficient preprocessing of the raw data with the instance frequency revolution; the LSTM and Bi-LSTM's accurate parameters were enhanced considerably to over 80% in both the training and testing phases. Keshtegar et al. [36] conducted the combination of support vector regression (SVR) and response surface model to forecast the loading capacity of walls. This combining model showed that the ratio average of the predicted testing was 0.98, gained outstanding performance, at the same time, maintained superior calculated efficiency and ran in the short time.

Regarding the difference between deep learning and machine learning models, the deep learning models are deployed to sequential input data including LSTM, Bi-LSTM, and FFNN-BP models [37–39]; meanwhile, machine learning models such as SVR is considered as non-sequential or appropriate for estimated tasks following input features of the models [40–42]. Moreover, this study is the first to use both deep learning and machine learning methods with four models to study and predict the displacement of the diaphragm wall in HCM City. At the same time, displacement data of underground works are time series data but do not follow certain rules (for example, seasonality such as weather data), and the input and output variables do not

belong to standard distribution. Hence, these proposed models will give forecast results with a high degree of accuracy.

This study suggests a dynamic estimation algorithm to investigate the excavation-induced concrete diaphragm wall deflection. The monitoring of wall deflection conditions was carried out to collect a valuable and faithful dataset. The generalization and applicability of four models containing Bi-LSTM, LSTM, FFNN-BP, and SVR are executed. After that, the highlight comparisons among the four models are based on the values of statistical accuracy parameters such as mean, standard deviation (SD), correlation coefficient (CC), kurtosis (Kurt), skewness (Skew), minimum (Min), maximum (Max), root mean square error (RMSE), mean absolute error (MAE), and mean absolute percentage error (MAPE). Simultaneously, the optimal performance model is given as a practical method for calculating the wall deflections. The findings may serve as a timely reminder to field stakeholders.

The next sections of the study continue as follows: in Section 2, the FFNN-BP, LSTM, Bi-LSTM, and SVR predicted algorithms are described, along with the implementation evaluation accuracy parameters. Next, in Section 3, a reality excavation construction is approved to evaluate the proposed estimation algorithms' applicability. Following that, the study outputs of four forecasting algorithms are evaluated and discussed in Section 4. Finally, the highlighted conclusions obtained from the experiments are sought in Section 5.

2 Study area, data acquisition, and methodology

2.1 The project site's description

A project namely the Opal Skyview building was constructed in Quarter 9, Hiep Bin Chanh Ward, Thu Duc Town, HCM City. Its scale got a land-use area of about 1,479 m². The project construction was estimated at around 30,942 m² including 21 floors and 2 basements. Figures 1 and 2 show the layout and cross-section of the deep excavation which was non-rectangular in shape. The deep excavation was supported by the 15 and 18 m bored pile retaining walls as well as two levels of steel struts. In addition, the soil–cement columns were used to reinforce the foundation below the basement. The maximum excavation depth was 8.9 m, which is located in SID2, while SID1 was excavated to a depth of 8.2 m. The horizontal displacements

of the deep excavations were monitored by the six inclinometers which were installed in the retaining wall as shown in Figure 2. In addition, the data in Table 1 show that the geology at the construction site consists of six layers of soil with the thickness of each layer as follows: soft clay 1 with 13 m, soft clay 2 with 7 m, soft clay 3 with 7 m, silt clay with 1.5 m, clay with 3.5 m, and medium dense sand (MDS) with 18 m, respectively.

2.2 Data acquisition

Regarding deep excavation works, data are usually collected to evaluate the displacement of the bore pile retaining wall, including the inclinometer depth (depth), implementation time for excavations (day), and the horizontal wall deflection. Monitoring data were collected at six inclinometers during the excavation period of 139 days, with the wall displacement measurement depth from 0.5 to 22 m (the scale distance is 0.5 m) and 42 monitoring cycles of collected wall deflection. Therefore, the input data of the study are 42 samples including depth, cycle, and date; the output data are the horizontal wall deflections. The distribution of the input and output wall deflection variables is presented in Figure A1. Moreover, the kernel density estimation (KDE), which is a non-parametric method to predict the probability density function of a random variable [43,44], and empirical cumulative distribution function (ECDF), which supplies a method for cumulative probabilities of the model and sample that the sample data cannot fit a standard probability distribution [45,46], describe the columns, curves, and fitted distribution curves of input and output variables in these figures. In addition, the KDE and ECDF methods also indicated that all input and output variables do not belong to the standard distribution. The statistical characteristic of the wall deflection variables in Table 2 indicates that the characteristics' range was computed from the observation of six locations, namely the mean, SD, Min, Max, Kurt, and Skew values. The mean and SD of the six SID locations were 21.25 and 13.53, 34.94 and 28.92, 31.02 and 21.36, 29.22 and 20.24, 26.98 and 20.06, and 28.09 and 18.48 mm, respectively. The Kurt and Skew values ranged from -1.39 to 0.03 and approached 0; these data could examine to accept for estimation. In addition, negative values for the skewness indicate skewed left data, and positive values for the skewness indicate skewed right side of data [47,48].

Mention about, the lines in Figure 3 yield the maximum the wall deflection induced by the excavation of six SID locations, namely 43.14 mm (at day = 110, depth =

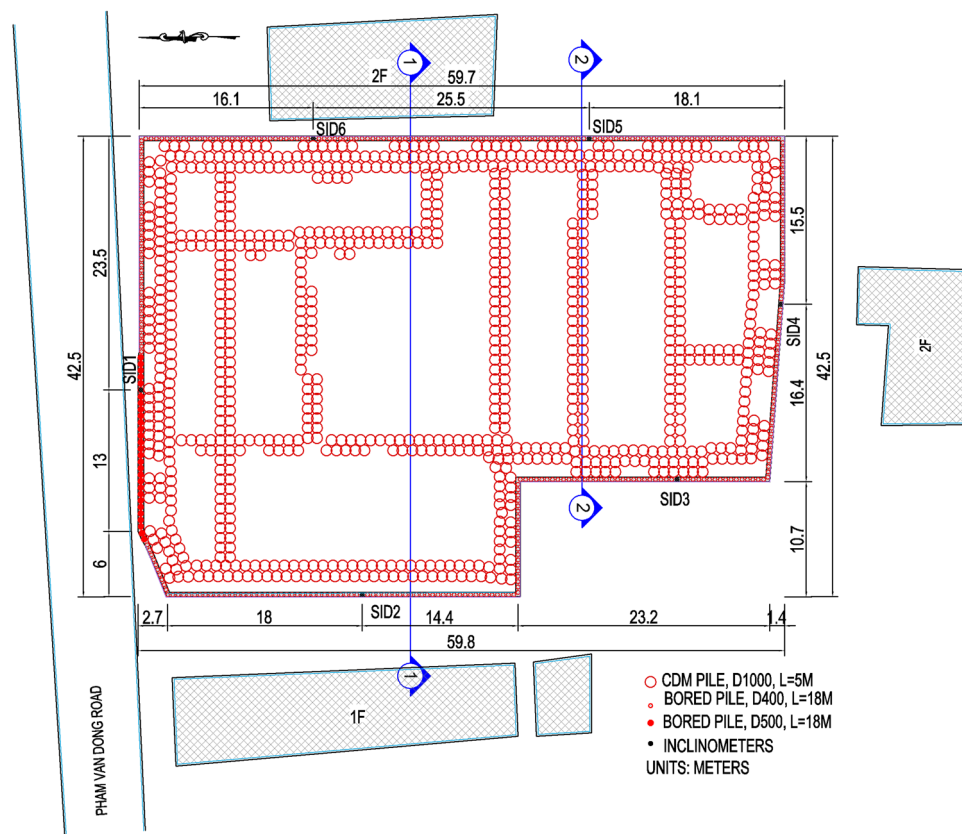


Figure 1: Plan view and instrument layout of deep excavation (unit: m).

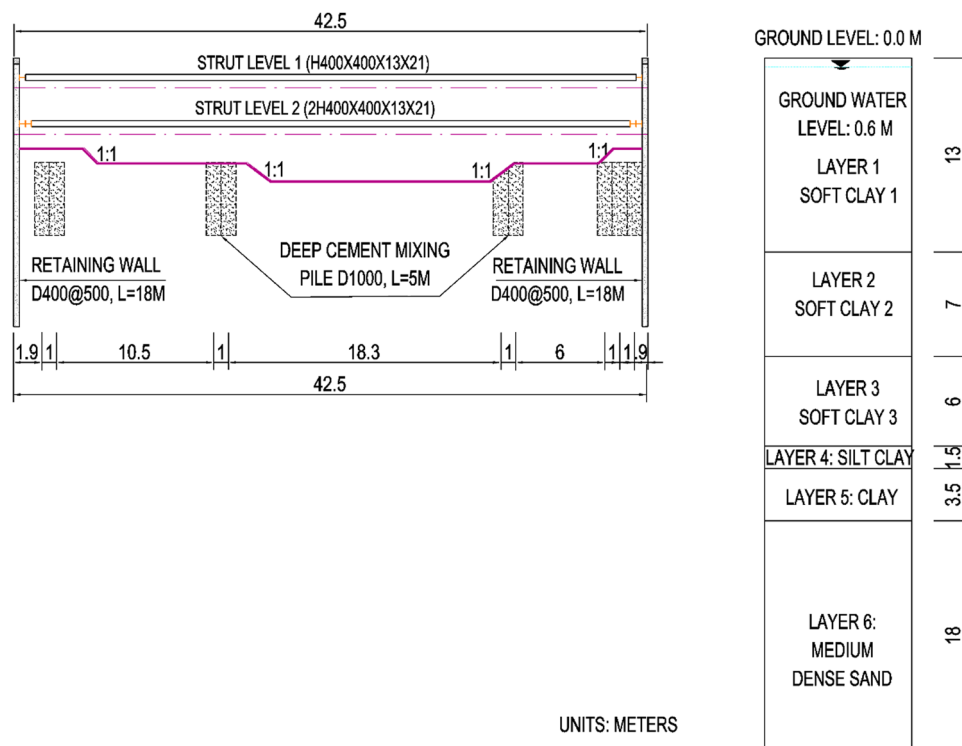


Figure 2: Cross-section of deep excavation: Sections 1-1 (unit: m).

Table 1: Synthesize soil parameters

Soil layer	Soft clay 1	Soft clay 2	Soft clay 3	Silt clay	Clay	MDS
Thickness (m)	13	7	7	1.5	3.5	18
γ_{unsat} (kN/m ³)	14.2	14.2	14.2	19	19.15	19.1
γ_{sat} (kN/m ³)	16.2	16.2	16.2	19.5	19.45	20.34
C (kN/m ²)	9	11	15	9.1	26.4	3.2
$\phi^{(0)}$	25.6	25.2	25	18	13.8	26
E'_{50}^{ref} (kN/m ²)	4,430	5,681	7,232	28,348	34,095	31,500
$E'_{\text{oed}}^{\text{ref}}$ (kN/m ²)	2,215	2,990	3,806	16,675	20,056	21,000
$E'_{\text{ur}}^{\text{ref}}$ (kN/m ²)	13,069	16,147	20,554	83,375	100,280	63,000
Drained type	U(A)	U(A)	U(A)	U(A)	U(A)	D

Table 2: Statistical characteristics of wall deflection data

Location	Mean (mm)	SD (mm)	Min (mm)	Max (mm)	Kurt	Skew
SID1	21.25	13.53	0.13	43.14	-1.39	-0.06
SID2	34.94	28.92	0.10	92.98	-1.02	0.58
SID3	31.02	21.36	0.11	66.94	-1.39	0.11
SID4	29.22	20.24	0.14	65.96	-1.29	0.19
SID5	26.98	20.06	0.10	66.44	-1.08	0.39
SID6	28.09	18.48	0.13	58.54	-1.38	0.03

-5 m), 92.93 mm (at day = 125, depth = -7 m), 66.94 mm (at day = 125, depth = -5 m), 65.96 mm (at day = 125, depth = -7.5 m), 66.44 mm (at day = 125, depth = -8.5 m), and 58.54 mm (at day = 131, depth = -8.5 m) occurred in SID1, SID2, SID3, SID4, SID5, and SID6, respectively; the plot also indicates the minimum the wall deflection to record at day = 5, and depth = -22 m of SID1, SID2, SID3, SID4, SID5, and SID6 locations are 0.13, 0.10, 0.11, 0.14, 0.10, 0.13 mm, respectively. The points are significant to note that the maximum deformations' position negatively impacts the wall depth and makes long-term deflection in the space dimension. In addition, the data in this figure have a maximum deflection achieved at depths from -5 to -8.5 m, and the time to peak is also from day 104 to day 139 of the deflection cycle measurement. This phenomenon shows that the correlations of the data of these locations are almost a weak relationship such as SID1, SID2, SID4, SID5, and SID6; two pairs SID1 and SID5 and SID3 and SID5 are negative correlations with correlation coefficients of -0.7 and -0.88, while three pairs namely SID5 and SID6, SID1 and SID3, SID4 and SID5 have strong relationship with correlation coefficients of 0.83, 0.76, and 0.60, respectively (details in Figure 4).

Before simulating models, the normalized database improves integrity and decreases redundancy. The database calibration using a Min-Max scaler normalization

(detail in Figure 5(a) and (b)) showed that the peaking wall deformation was observed in the 42 recorded samples. The calibration data were divided into 32 samples (from 1st to 32nd) and 10 samples (from 33rd to 42nd) for training and testing (validation verification) phases. Furthermore, the models' estimation indicated an excellent regression level if it achieves implementation on datasets outside the training samples. Hence, this study deployed a walk-forward validation (WFV) technique to evaluate the generalization ability of the models' estimation. WFV for time series data was developed by Pardo [49]. The WFV methodology is used only for a fixed number of observations and demonstrates the estimating model with the best chance to get a good prediction at each time step. First, using historic data (cycle) for training, the forecasting model does a load prediction for the next day (cycle 1), then assessed against the previous value. Continuously, the training data are expanded to include the previous value (cycles + cycle 1). The process is looped to the end to ensure that the training data were updated with the unknown values at each step [50]. In addition, the numbers of the splits for walk-forward validation technique were 3 (Figure A2).

2.3 LSTM model

The LSTM is considered a deep neural network constructed to handle data having order properties. The data in Figure 6 show the basic structures of the LSTM [51–53]. The LSTM neuron has two statuses, namely cell status $C^{(t)}$ consisting of long-term memory and hidden status $h^{(t)}$ consisting of short-term memory, where new data are carefully verified using three “gate” modules. In the long-term series, the “gate” modules efficiently tackle the gradient vanishing issue. The gate signal ranges from 0 to 1, with 0 indicating that all input data should be ignored and 1 indicating

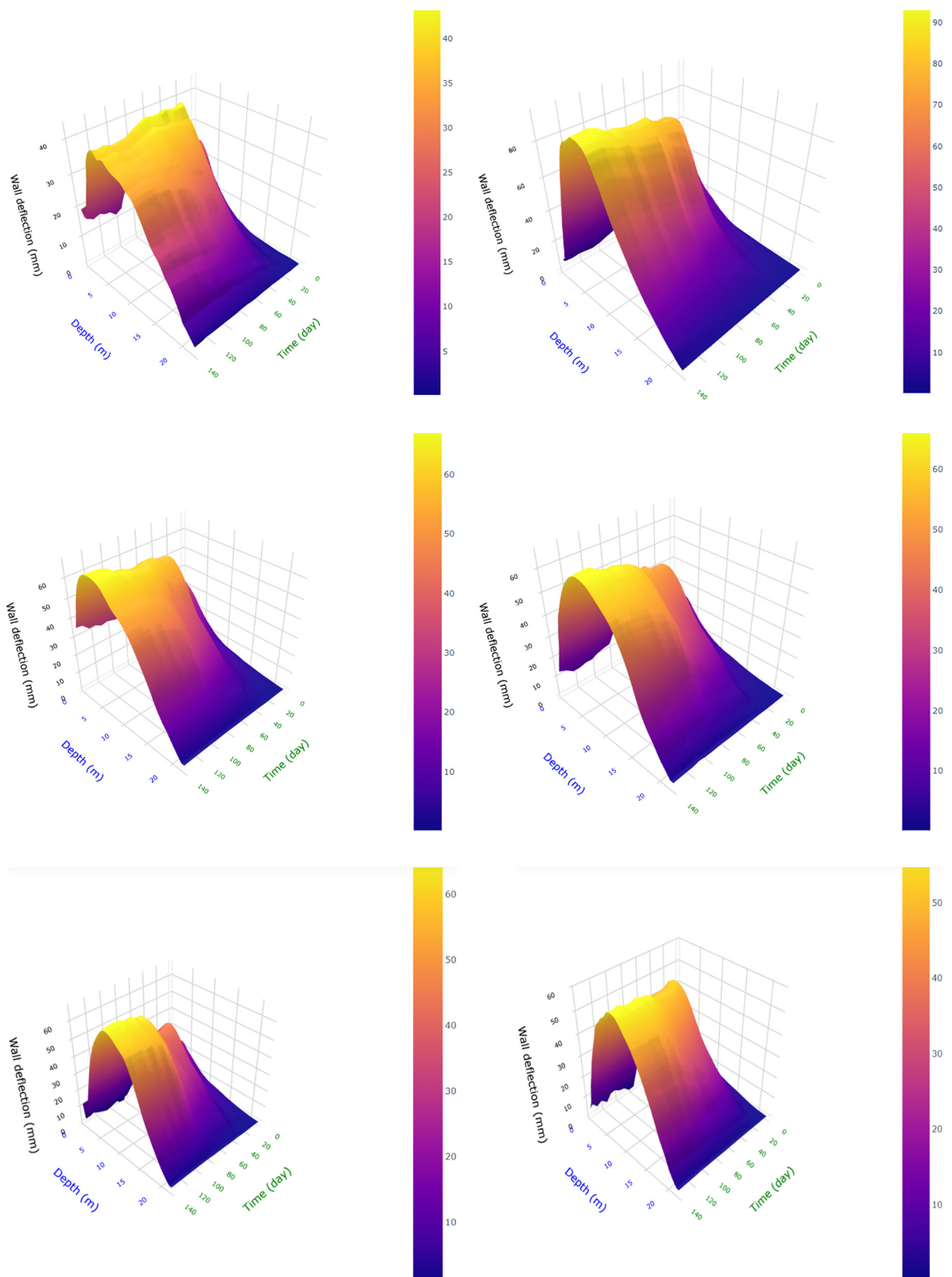


Figure 3: Observations of the wall deflections for inclinometers following depth and time.

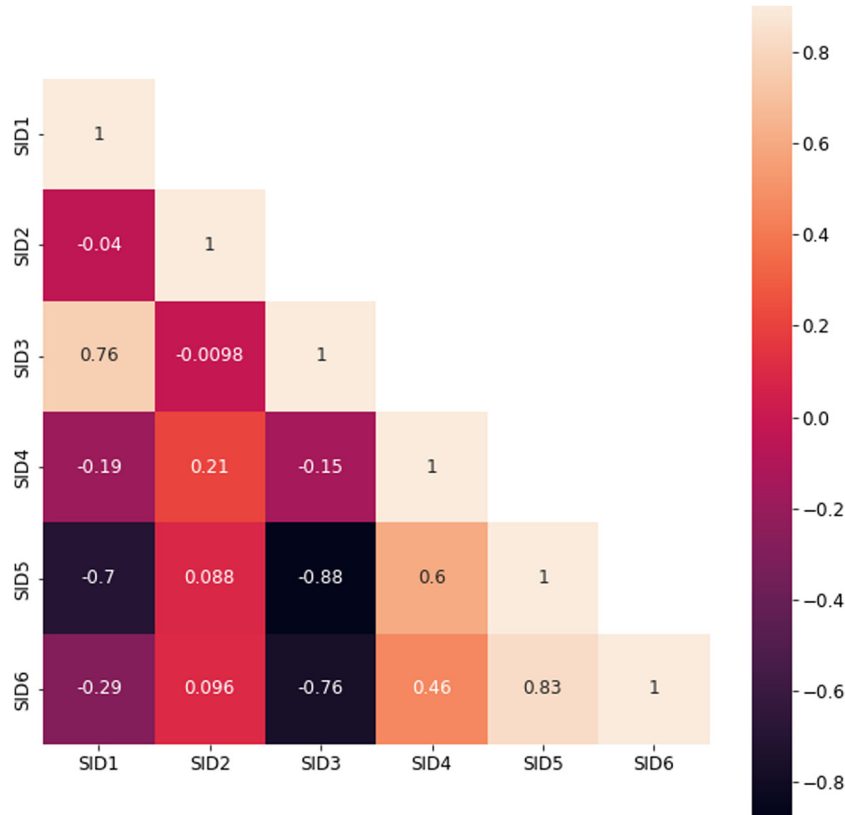


Figure 4: The correlation among six SID locations.

that all new information is extremely important and could be remembered.

The forget gate, symbolized as $f^{(t)}$, is used to estimate the cell status' forget ratio at the time t , which can be estimated using the following equation:

$$f^{(t)} = \sigma(W_f[h^{(t-1)}, x^{(t)}] + b_f), \quad (1)$$

$$i^{(t)} = \sigma(W_i[h^{(t-1)}, x^{(t)}] + b_i), \quad (2)$$

$$\tilde{C}^{(t)} = \tanh(W_C[h^{(t-1)}, x^{(t)}] + b_C), \quad (3)$$

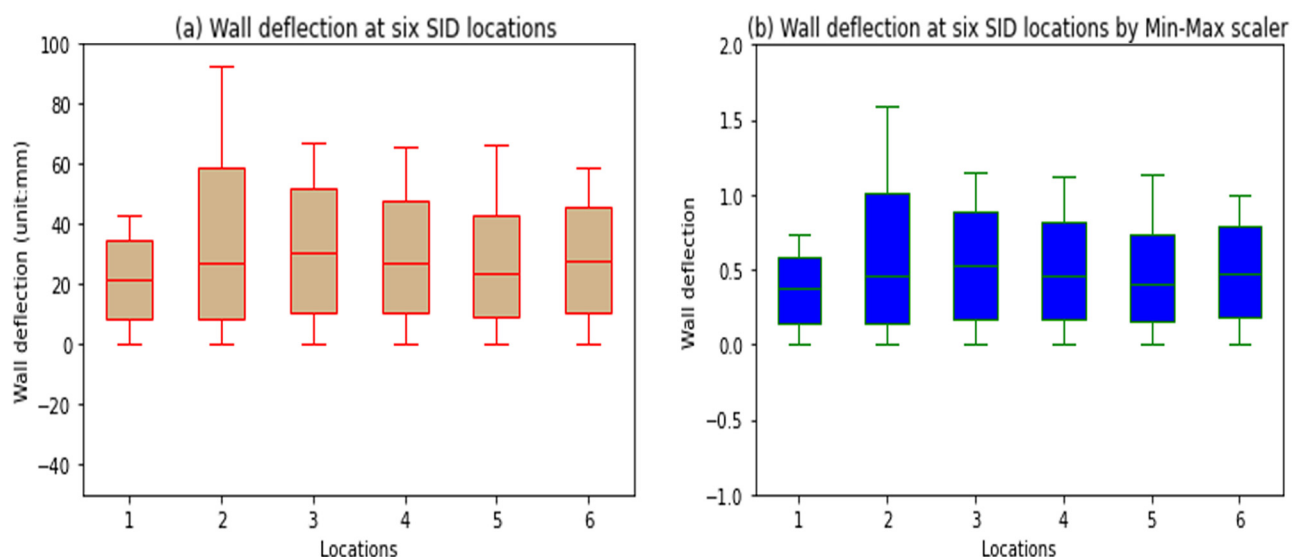


Figure 5: (a) Calibration vector of the wall deformation and (b) calibration vector of the transformed the wall deformation using Min-Max scaler.

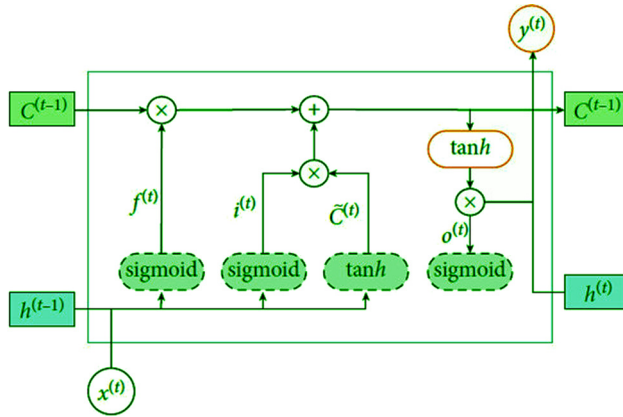


Figure 6: Schematic view of the LSTM neuron [54].

$$C^{(t)} = f^{(t)} \cdot C^{(t-1)} + i^{(t)} \tilde{C}^{(t)}. \quad (4)$$

The input gate is, expressed as $i^{(t)}$, estimates the new information's proportion to be added to the cell status, which is represented in equation (2).

The output gate is denoted as $o^{(t)}$, which analyzes the output and updates the hidden status.

$$y^{(t)} = \sigma(W_o \cdot [h^{(t-1)}, x^{(t)}] + b_o), \quad (5)$$

$$h^{(t)} = o^{(t)} \cdot \tanh(C^{(t)}), \quad (6)$$

where $\tilde{C}^{(t)}$ is the LSTM neuron's candidate cell status at the time t ; W and b symbolize weight and bias terms, respectively; σ is the sigmoid's activation function; and \tanh is denoted as the hyperbolic tangent's activation function. The optimal model with the values of the core parameters of the LSTM input size are 42 nodes, and layer has 500 hidden nodes that map the input time series to 500 features before sending the output to the fully connected layer, which has 01 output node. Following that, the activation function for each hidden layer is \tanh function; Adam optimization is a stochastic gradient descent method; the function of performance is MSE; the number of epochs is 200; and the batch size is 50.

2.4 Bi-LSTM model

The Bi-LSTM network is a more advanced form of the LSTM algorithm. Bi-LSTM is made up of two hidden layers that work in both forward and backward directions. Because the Bi-LSTM network can learn and use both past and future information at any point in time, this architecture can increase model operation. This study established Bi-LSTM network structures as shown in Figure 7 [53,55,56]. For time-sequential data, one input node is included. The optimal values of the model's core parameters are similar to the LSTM model.

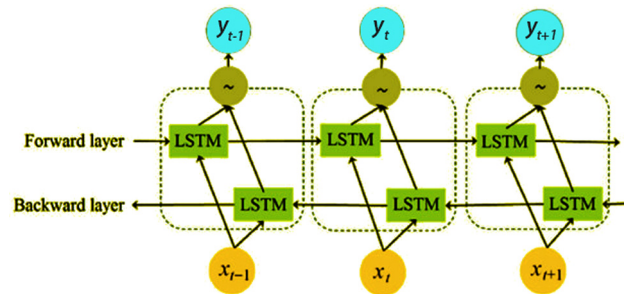


Figure 7: Schematic view of the Bi-LSTM neuron [55].

2.5 FFNN-BP model

FFNN-BP algorithm is considered a family of neural network methods [57]. It can describe arbitrarily complex nonlinear processes for any system regarding inputs and outputs. Its structure in Figure 8 consists of a three-layer neural network such as an input layer, hidden layer (layers), and output layer [58,59]. The input layer includes 42 input nodes from i_1 to i_{42} , 01 output nodes named o in the output layer have represented the values of wall deflection points. There are three hidden layers; the first hidden layer consists of neurons from H_{11} to $H_{1,200}$, the second layer includes neurons from H_{21} to $H_{2,200}$, and the third layer compounds neurons from H_{31} to $H_{3,200}$. Each neuron of the hidden and output layers conducts a corresponding weight and bias, as w_{11}^2 , $B_1^{(2)}$ and w_{12}^2 , $B_2^{(2)}$ are the weight and bias to represent for neurons of H_{11} and H_{12} , so on. In order to compare anticipated outputs with known outputs, the weight and bias values can be assigned gradually and corrected during the training process; backpropagation method for train networks [59]. Each neuron of the hidden layers achieves the output from all neurons of the previous layers and converts these values with a weighted linear sum into the output layer. The output layer gets the values from the last hidden layer. The \tanh function is deployed as the activation function for the three hidden layers. The Adam method is considered stochastic optimization to the solver of weight optimization; the function of performance is MSE; the number of epochs are 200; and the batch size is 50.

2.6 SVR model

The SVR model is deployed to look for an appropriate hyperplane in higher dimensions to be suitable for the data with an acceptable threshold error 2ε [60]. The model is also widely applied in regression task. The acceptable

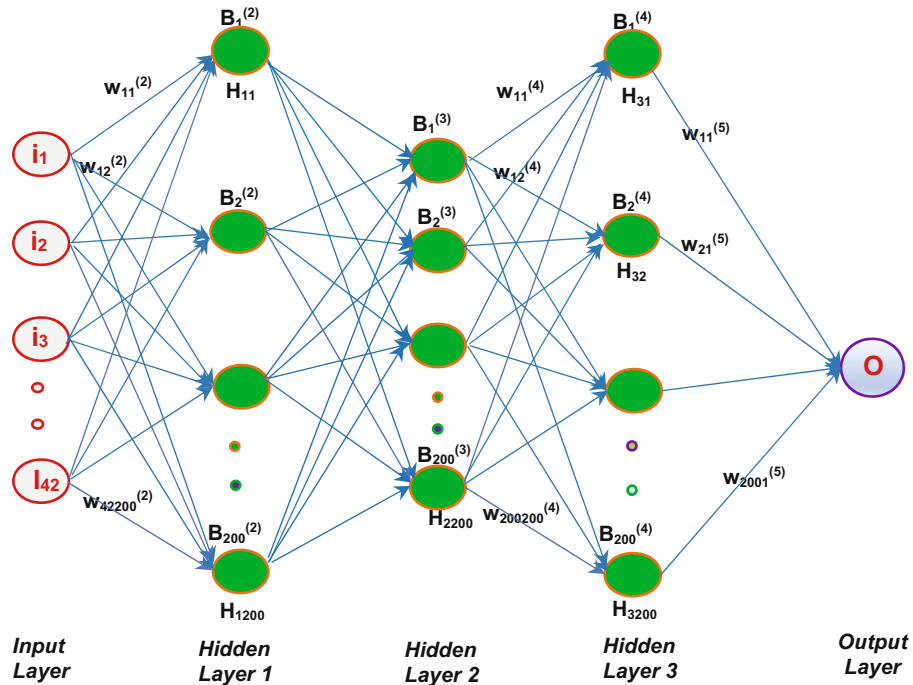


Figure 8: Structure of FFNN-BP network.

threshold error is 2ϵ ; this value is the distance from the hyperplane to the boundary line (detail in Figure 9) [36,61]. In this study, the optimum parameters for the model are the following: value of ϵ is 0.01; kernel function is radial basis function; and hyperparameter C is 1,000.

2.7 The data normalization

The accurate estimation of the wall deformation induced by excavation based on LSTM, Bi-LSTM, and FFNN-BP

requires dimensionless data processing. Therefore, this study deploys the approach of Min-Max normalization for this research. The Min-Max normalization is a linear transformation approach, also well known as the normalization deviation, which leads the result to fall within the range [62–64]. The following is the conversion formula:

$$\hat{Y} = \frac{Y - \min}{\max - \min}, \quad (7)$$

where Y and \hat{Y} are the original and normalized data, and min and max are the original sample data's minimum and maximum values.

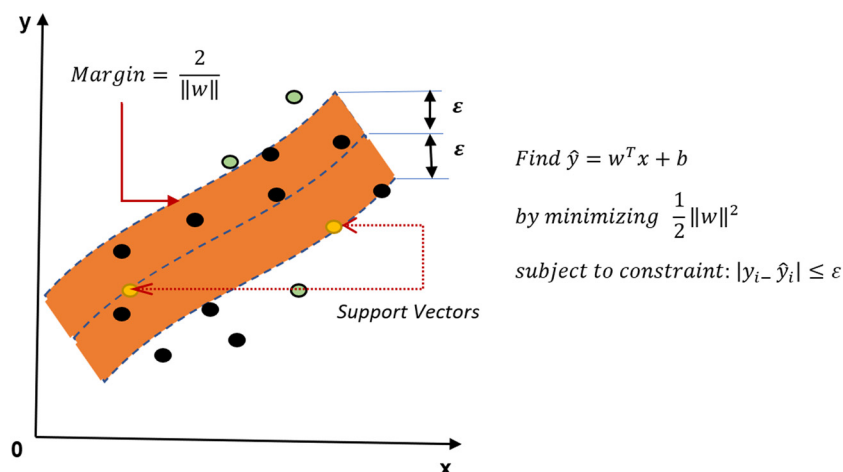


Figure 9: Structure of SVR model [60].

2.8 Performance metrics

Predicting outputs relies on calculating and comparing the actual data to the estimated ones. These metrics of the accuracy measurement indicators consist of the MAPE, RMSE, MAE, and CC. At the same time, the error metrics are defined as follows [65,66]:

$$\text{MAPE}(\%) = \frac{1}{n} \sum \frac{|x'_t - x_t|}{x_t} \%, \quad (8)$$

$$\text{RMSE} = \sqrt{\frac{\sum_{t=1}^n (x_t - x'_t)^2}{n}}, \quad (9)$$

$$\text{MAE} = \frac{1}{n} \sum_{t=1}^n |x'_t - x_t|, \quad (10)$$

$$\text{CC} = \frac{\sum_{t=1}^n (x_t - \bar{x})(x'_t - \bar{x}')}{\sqrt{\sum_{t=1}^n (x_t - \bar{x})^2} \sqrt{\sum_{t=1}^n (x'_t - \bar{x}')^2}}, \quad (11)$$

where x_t, x'_t are the predictive value and observed value in the period time t , n is the number of the observed data in

the testing stage, and \bar{x}, \bar{x}' are the mean of the estimated and observed values. The MAPE, RMSE, and MAE parameters can be as close to 0, and CC should be approaching 1 to indicate strong model performance as possible.

The process of the aforementioned experiment locations in this study is shown in Figure 10. First, the database is preprocessed and checked by statistical methods, and it is divided into training and testing sets. Second, the LSTM, Bi-LSTM, FFNN-BP, and SVR algorithms are used based on the training samples and the optimal parameters are collected. Finally, the four models' performances are compared using the accuracy measurement indicators as RMSE, MAE, MAPE, and CC in the possible result stage. To look for the best prediction values for models if the MAPE, RMSE, MAE approach the lowest values, and CC gain the highest; else, the experiments are adjusted by component indicators of models or training data size to find the optimal accuracy measurement parameters.

3 Results

This study conducts on prediction of the displacement of the retaining wall at Opal Skyview building, with the selection of input variables for all six SID locations kept the same as indicated in Figure 1 to warranty compatibility with the locations. At the same time, the four models named LSTM, Bi-LSTM, FFNN-BP, and SVR were used for predicting the horizontal wall displacements of deep excavation. The experiment result to find the best model for all analyzed SID locations are shown in Table 3. Following the collected results of simulations, four models indicate that the best estimation is at SID3, where the MAPE, RMSE, and MAE values of training and testing phases were the lowest in the established models. And the second best is the result at SID6. The lowest prediction result is at SID2. In addition, the remaining predicted values of SID1, SID4, and SID5 are between the values of SID2 and SID6. At the same time, the scatter charts for the testing and training phase in Figure 11(a–f1) show that the black triangles, green triangles, purple multiplies, and red pluses are marks of the SVR, Bi-LSTM, FFNN-BP, and LSTM, respectively. These marks also indicate that the black triangle is the nearest green line, and it means that the SVR model is the best appropriate of the other models at all locations. The second-nearest, third-nearest, and fourth-nearest are green triangles, purple multiplies, and red pluses, respectively. These points also reveal that the second-highest, third-highest, and fourth-highest forecasting scores are the FFNN-BP, BiLSTM, and LSTM models, respectively. In addition, this study has converted the data

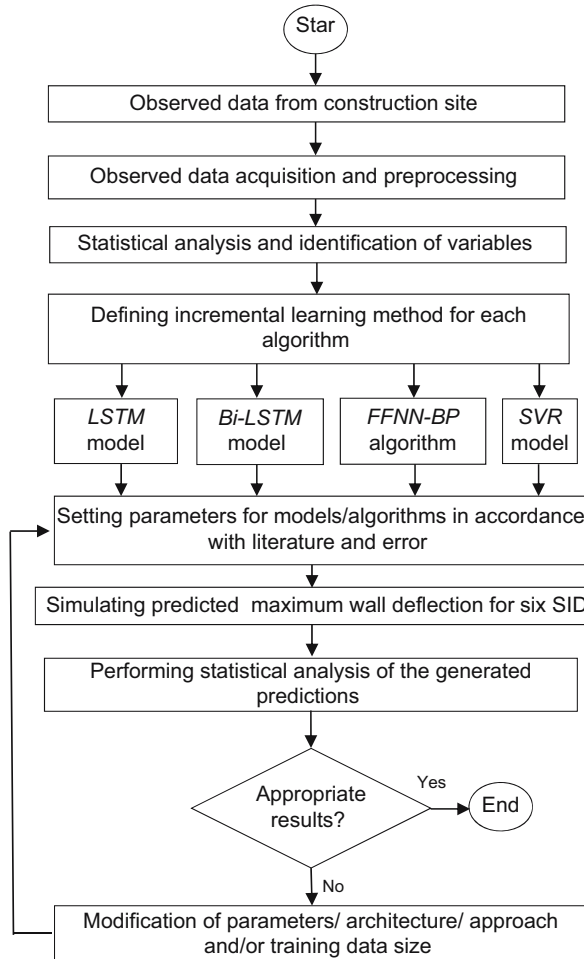


Figure 10: Flowchart of the research steps used in this study.

array of 42 cycles into an average dimension array of the actual/monitoring data and the predicted data in Figure 12; the green dot line, blue line, purple dash line, red dot line, and black line represent Bi-LSTM, FFNN-BP, SVR, LSTM predicted data, and actual wall deflection data, respectively. The lines in Figure 12 show that the blue line and purple line are closer black line than the red line. In other words, the predicted result of the SVR, FFNN-BP, and Bi-LSTM models fitted than the LSTM model. These points impress that the SVR, FFNN-BP, and Bi-LSTM models have indicated engaging capability in retaining wall problems. In terms of examining the deformation prediction model, the optimal model from the selected walk-forward cross-validation is obtained to estimate six measuring points shown in Figure 1.

Regarding assessing outperforms of the four models for forecasting bore pile retaining deflection, this study use Taylor diagram to compare the outperform. It may be considered that the visual description of the Taylor diagram summarizes plentiful aspects of the algorithm and observed indicators. In the diagram chart, the radial distance is used to present the standard deviation, and the correlation between the estimation and measurement is shown by the azimuthal angle of the predicted field. Furthermore, Taylor diagrams may also highlight the

goodness models to compare to that of observations where the diagram chart can visualize plenty of points on a polar plot. The plots in Figures 13 and 14 describe the SD and CC between the datasets of observation, and prediction for six SID locations are indicated in the Taylor diagram. From the data in the figures, it may be observed that the CC approach up to 1. These points prove the algorithms are overall consistent between the actual and predictive values. It is clear that the Taylor diagram demonstrates the optimal models with the highest accuracy. Hence, it will result in overestimation when the SD of the predicted values is higher than the SD of observed values and vice versa. Among the four models, SVR, Bi-LSTM, and FFNNBP models present the highest correlation. Meanwhile, LSTM shows the lowest implementation in wall deflection estimated tasks, displaying the longest distance to the measurement point.

4 Discussions

The proposed research project is located in very thick soft ground layers of HCM City, Vietnam, so the basement of the

Table 3: Accuracy parameters for the prediction of the wall deflection

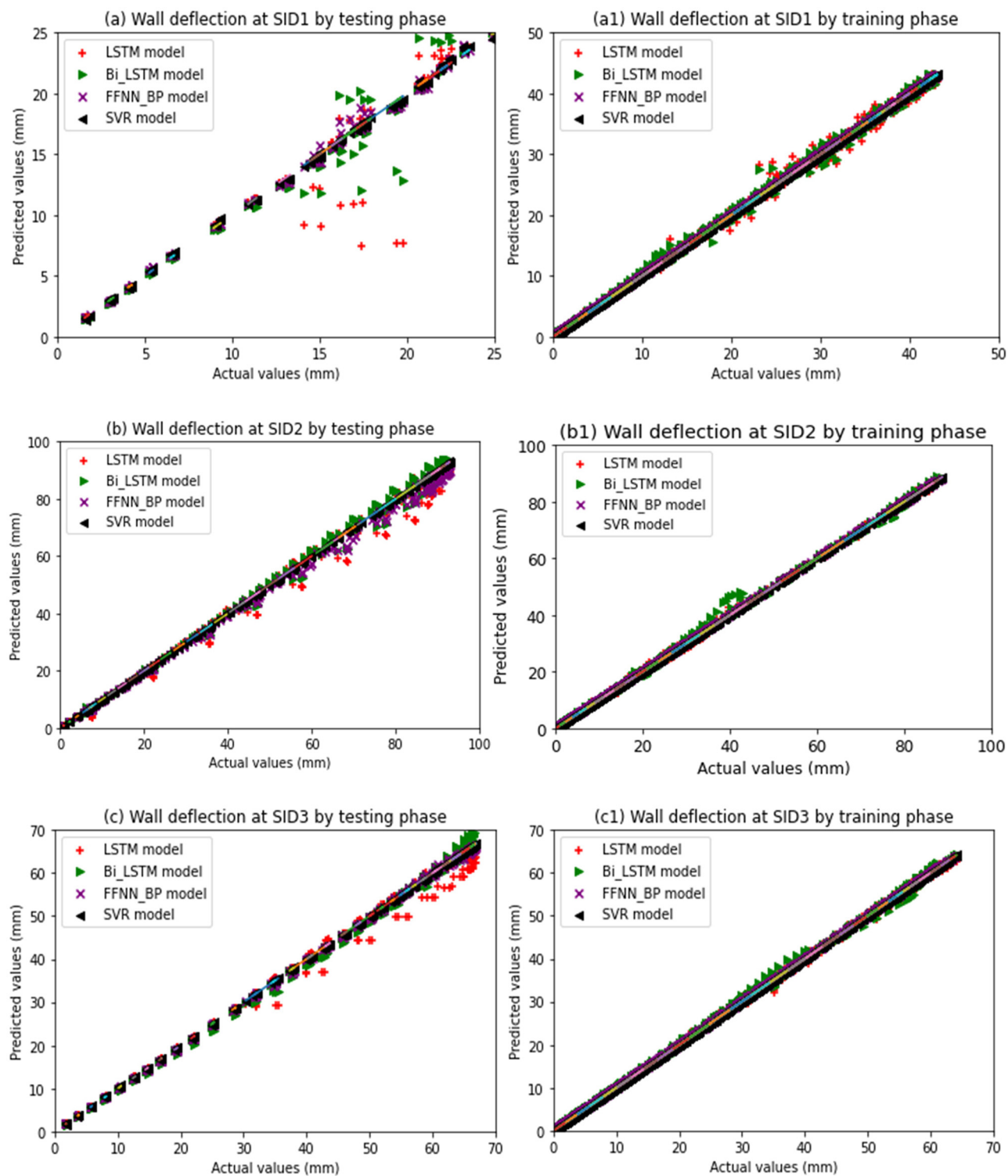


Figure 11: The actual and predicted wall deflection at testing and training phases based on the four models in (a, a1) SID1, (b, b1) SID2, (c, c1) SID3, (d, d1) SID4, (e, e1) SID 5, and (f, f1) SID6 locations.

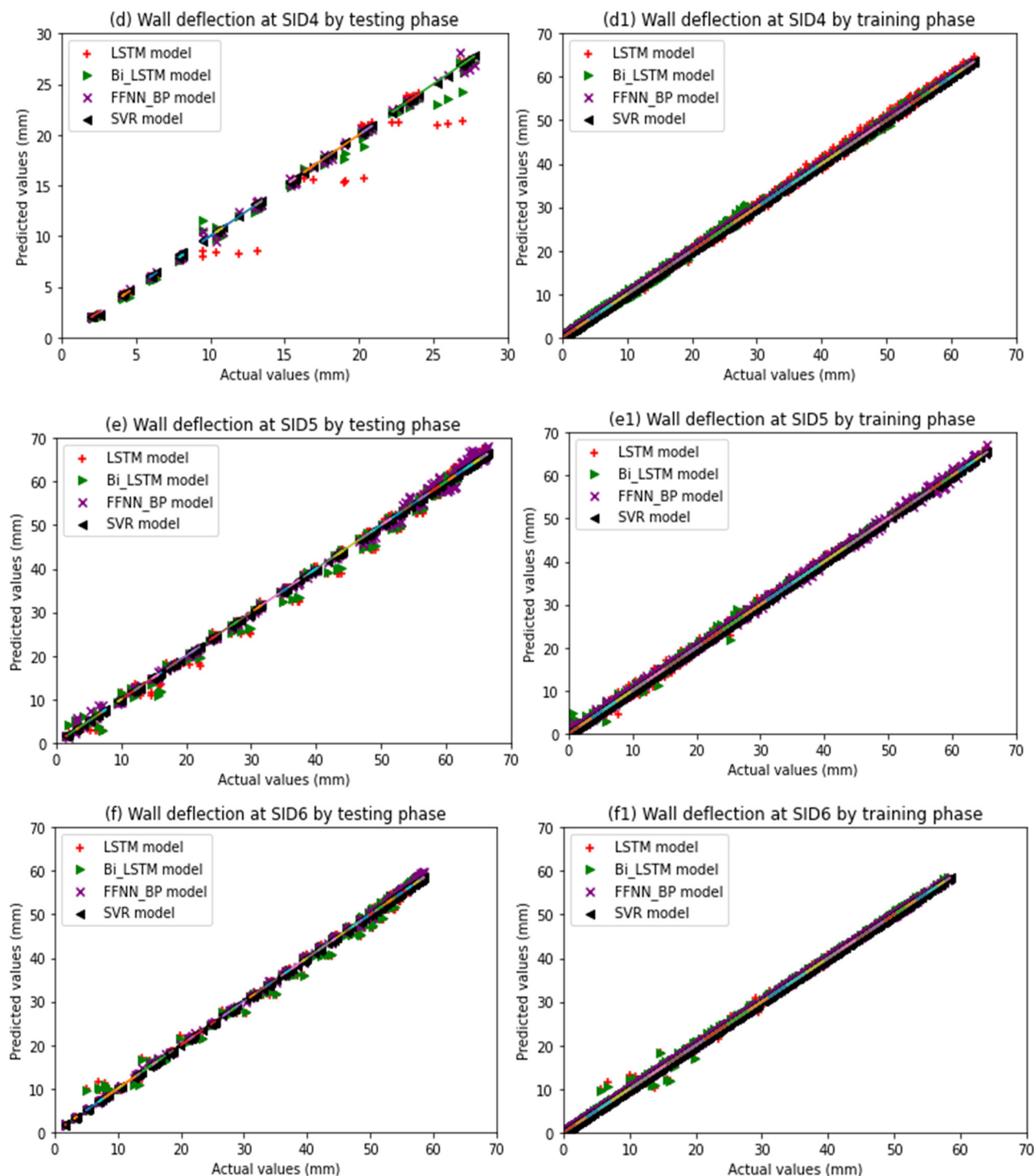


Figure 11: (Continued)

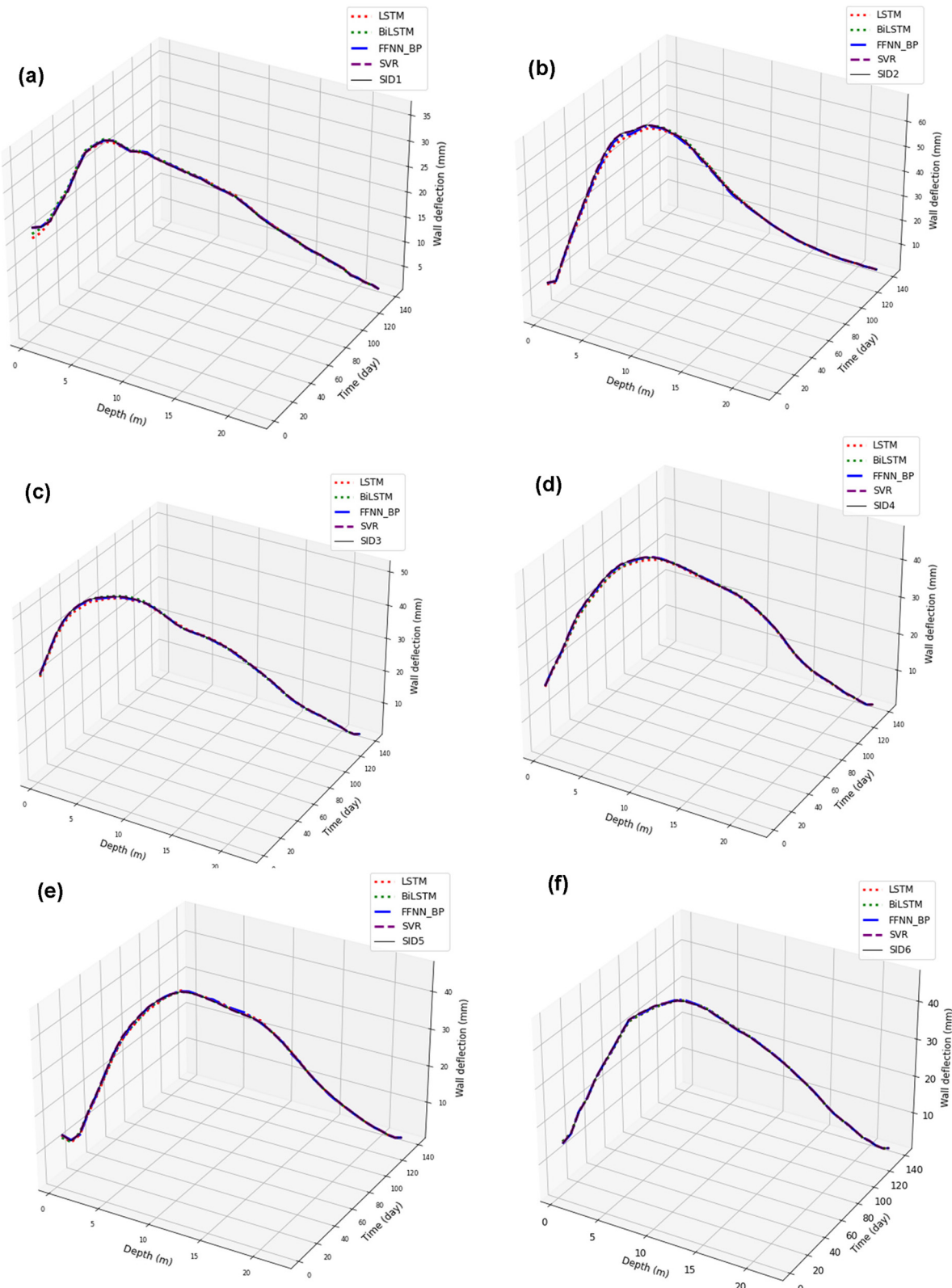


Figure 12: The actual and predicted average of wall deflection based on the four models in (a) SID1, (b) SID2, (c) SID3, (d) SID4, (e) SID5, and (f) SID6 locations.

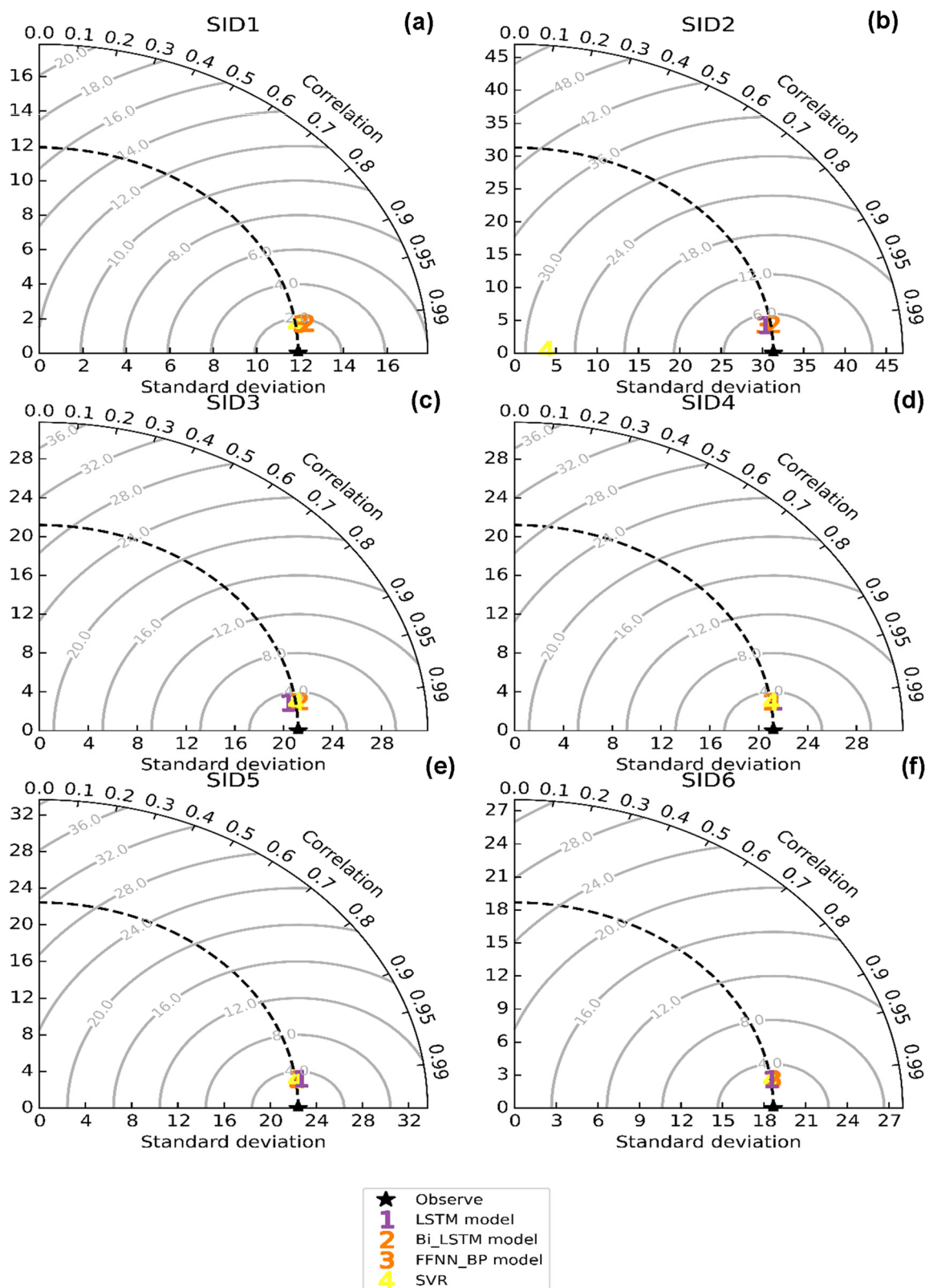


Figure 13: Taylor diagram presenting the best testing performance of LSTM, Bi-LSTM, FFNN-BP, and SVR models of (a) SID1, (b) SID2, (c) SID3, (d) SID4, (e) SID 5, and (f) SID6 locations.

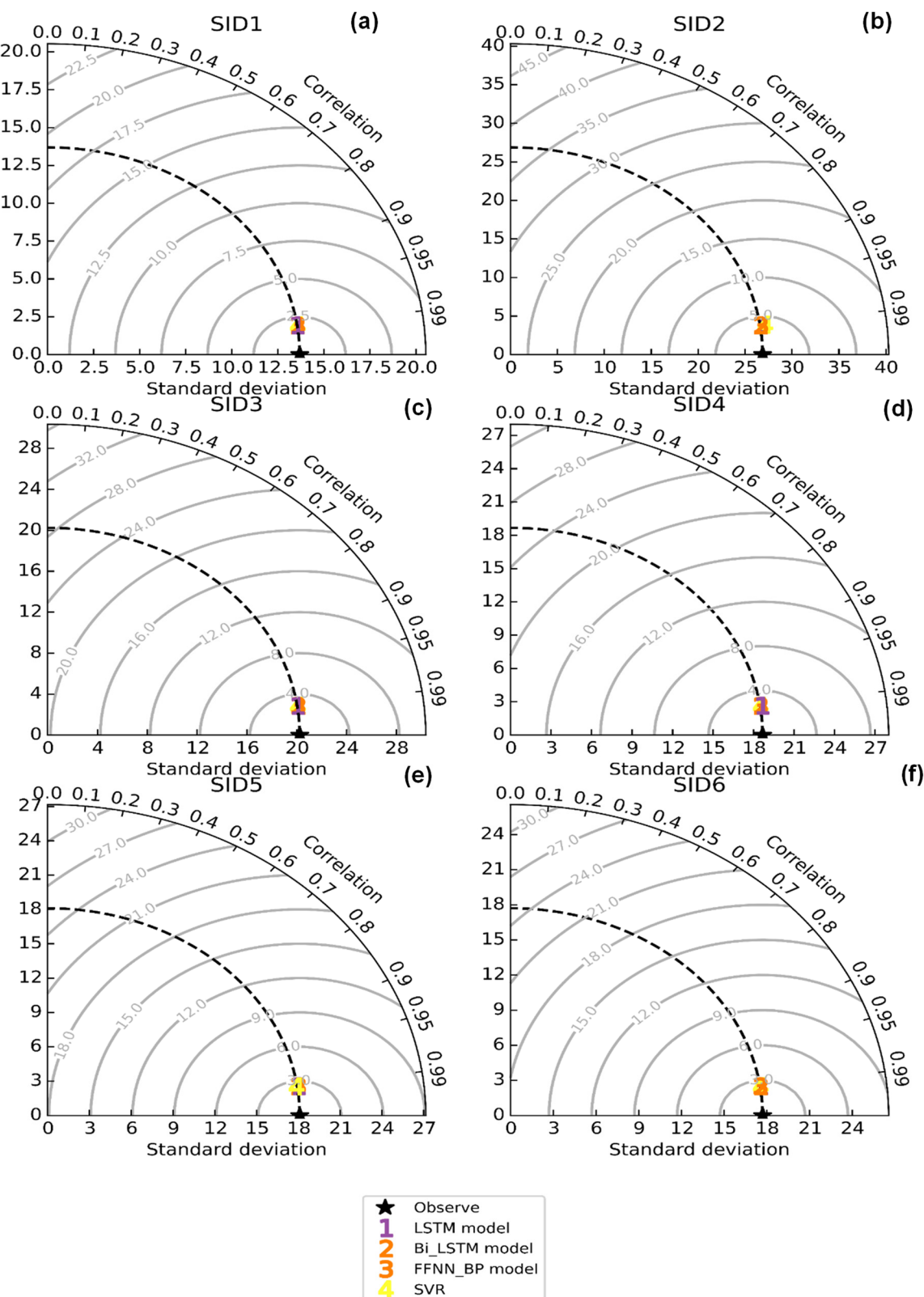


Figure 14: Taylor diagram presenting the best training performance of LSTM, Bi-LSTM, FFNN-BP, and SVR models of (a) SID1, (b) SID2, (c) SID3, (d) SID4, (e) SID 5, and (f) SID6 locations.

high-rise building herein was retained by the bored pile retaining walls to improve the safety of excavation during construction. It is aware that predicting the wall deflection of deep excavation is very crucial to promote the understanding of the deep excavation behavior as well as prevent any unexpected incidents during construction stages. Therefore, this study suggests four models of LSTM, Bi-LSTM, FFNN-BP, and SVR for predicting the wall deflection for deep excavation in soft ground. With data on the displacement of the retaining wall carried out over 139 days and 42 cycles, the experiment results show that the main prediction tasks consist of the feasible testing performance and the usable capacity of the algorithms. Four proposed methods indicated the precise progression of observation and estimation tasks. All RMSE, MAE, and MAPE values were lower than 2.16 mm, 1.86 mm, and 0.12 mm, respectively; these points demonstrate that the methods are acceptable in engineering practice. In the space aspect, the four models' prediction results indicate excellent appreciation of the reality deformations in different locations of excavation. In addition, these models may accurately know the location of maximum lateral deformation along with the wall depth. At the same time, the study result also indicates that BiLSTM, SVR, the Bi-LSTM, SVR, and FFNN-BP models outperform the LSTM model in the prediction results' retaining wall deviation.

In terms of evaluating these models' predicted accuracy, the results of this study compared with the other study results. For instance, Zhao et al.'s study [4] about diaphragm wall deformation prediction induced by excavation indicates the BPNN model with $MAE = 13.89$ mm, $MAPE = 53.27\%$ and LSTM model with $MAE = 1.79$ mm and $MAPE = 7.99\%$. The predicted indicators of LSTM are equivalent with this study's LSTM model; however, the FFNN-BP model's estimating parameters are higher than this study. Ma et al. (2022) [49] used LSTM to estimate tunnel deformation in high *in-situ* stress regions. The result indicated that MAE and RMSE values for the testing phase were 0.20 and 0.19, respectively. The values of accuracy parameters are as equivalent as these study results. Elnabwy et al. [67] used the SVR model to predict sedimentation quantities and access their performance. The result pointed out that RMSE for the training phase = 1.35 and RMSE for the testing phase = 2.10; the values are the same as RMSE of this study.

Although this study was conducted in a high-rise building on the weak ground areas around the city and the number of samples was only 42 for each location, the testing and training phase results also point out that the values of prediction data were consistent with monitoring data. This study has implemented three activation functions such as ReLU, Sigmoid, and tanh to choose for the

deep learning model, but the best activation function was the tanh function. However, this study has not applied the tanhLU function to deep learning models because this activation function promises to potentially replace tanh for neural networks [68]. Moreover, the degree of displacement of the retaining wall during construction is within allowable and safe limits. This project also shows that the construction units and design consultants have performed in accordance with the requirements of the investor.

5 Conclusions

This study used deep learning and machine learning algorithms such as the LSTM, Bi-LSTM, FFNN-BP, and SVR models to predict the wall deflection for deep excavation in soft ground. This prediction was performed based on the database of *in situ* measurements collected from a real-life excavation project. The results of the proposed method indicate the following:

The study area's geotechnical characteristics included a soft clay layer covering 63% of the subsoil and the wet-sand layers were inside and below the deep excavation depth range of the project. The subsoil conditions indicate that excavation activity could be dangerous.

The results indicated widely deployed performance indicators such as MAPE, RMSE, MAE, and CC. At the same time, the obtained results of the algorithms proved the highest accuracy of SVR at six SID locations, and the second-highest, third-highest, and fourth-highest accuracies were FFNN-BP, Bi-LSTM, and LSTM, respectively.

The models gained high accuracy prediction and exhibited variation decrease and robustness tasks based on the walk-forward cross-validation.

These four algorithms proposed in this study support real-time safety reviewing and early warning conducted for wall deformation in the construction area.

There is a need for legal guidelines for the architecture of deep excavations in HCM City soft ground.

This study only focuses on one excavation; therefore, the result cannot be compared with others. In addition, the dataset for the modeling is not larger samples, and a more high-quality database could be generated urgently. At the same time, this study has not applied the tanh LU function to deep learning models because this activation function promises to potentially replace tanh for neural networks [68].

Acknowledgments: This research was supported by University-level project: "Predicting ground settlement caused by deep excavation works by artificial intelligence model," No.: 524/HD-NCKHPTCN of Thu Dau Mot University. PhuocThanh

Construction Company, No.21, 24 St., Him Lam Residential Area, Binh Hung Ward, Binh Chanh District, Ho Chi Minh City, Vietnam.

Funding information: This research is funded by Thu Dau Mot University, Binh Duong Province, Vietnam under grant number DT.20.2-052.

Author contributions: Data collection: KhacHai Phan, ThiTuyetNga Phu; conceptualization, methods, modeling: HongGiang Nguyen, DuyPhuong Le; writing, original draft preparation: DinhHieu Tran; ThiTuyetNga Phu, TienThinh Nguyen; writing, review, and editing: YuRen Wang, KhacHai Phan; funding acquisition: DinhHieu Tran, ThiTuyetNga Phu. All authors have read and agreed to the published version of the manuscript.

Conflict of interest: The authors declare no conflict of interest. The first author is authorized to use this article for his related study work.

Data availability statement: The data used to support the findings of this study are available from the corresponding author upon request.

References

- [1] Liu W, Shi P, Cai G, Gan P. A three-dimensional mechanism for global stability of slurry trench in frictional soils. *Eur J Environ Civ Eng.* 2022;26(2):594–619.
- [2] Mohamed AA. Effect of diaphragm wall construction on adjacent deep foundation. Germany: Geoengineering and Mining of the Technische Universität Bergakademie Freiberg; 2017.
- [3] Liu W, Shi P, Cai G, Cao C. Seepage on local stability of slurry trench in deep excavation of diaphragm wall construction. *Comput Geotech.* 2021;129:103878.
- [4] Zhao H, Liu W, Guan H, Fu C. Analysis of diaphragm wall deflection induced by excavation based on machine learning. *Math Probl Eng.* 2021;2021:1.
- [5] Liu W, Shi P, Li H, Wang F. Observed performance of three adjacent 48 m depth concrete diaphragm wall panels in silty soils. *Can Geotech J.* 2019;56(11):1736–42.
- [6] Zhu G. Mindlin solution on ground deformation caused by the trench excavation during installation of concrete diaphragm wall panels. *Sci Rep.* 2021;11(57):1–16.
- [7] Zhao HJ, Liu W, Shi PX, Du JT, Chen XM. Spatiotemporal deep learning approach on estimation of diaphragm wall deformation induced by excavation. *Acta Geotech.* 2021;16(11):3631–45.
- [8] Chen DP, Qian CX, Liu CL. A numerical simulation approach to calculating hygrothermal deformation of concrete based on heat and moisture transfer in porous medium. *Int J Civ Eng.* 2010;8(4):287–96.
- [9] Zhang QQ, Liu SW, Feng RF, Li XM. Analytical method for prediction of progressive deformation mechanism of existing piles due to excavation beneath a pile-supported building. *Int J Civ Eng.* 2019;17(6):751–63.
- [10] Mahin Roosta R, Alizadeh A. Simulation of collapse settlement in rockfill material due to saturation. *Int J Civ Eng.* 2012;10(2):93–9.
- [11] Elbaz K, Shen SL, Zhou A, Yin ZY, Lyu HM. Prediction of disc cutter life during shield tunneling with AI via the incorporation of a genetic algorithm into a GMDH-type neural network. *Engineering.* 2021;7(2):238–51.
- [12] Long M. Database for retaining wall and ground movements due to deep excavations. *J Geotech Geoenviron Eng.* 2001;127(3):203–24.
- [13] Xiao H, Zhou S, Sun Y. Wall deflection and ground surface settlement due to excavation width and foundation pit classification. *KSCE J Civ Eng.* 2019;23(4):1537–47.
- [14] Mei Y, Zhou D, Wang X, Zhao L, Shen J, Zhang S, et al. Deformation law of the diaphragm wall during deep foundation pit construction on lake and sea soft soil in the Yangtze River Delta. *Adv Civil Eng.* 2021;2021:Article ID 6682921.
- [15] Goh ATC, Zhang F, Zhang W, Zhang Y, Liu H. A simple estimation model for 3D braced excavation wall deflection. *Comput Geotech.* 2017;83:106–13.
- [16] Hsieh PG, Ou CY, Lin YL. Three-dimensional numerical analysis of deep excavations with cross walls. *Acta Geotechnica.* 2013;8(57):33–48.
- [17] Hsieh PG, Ou CY. Simplified approach to estimate the maximum wall deflection for deep excavations with cross walls in clay under the undrained condition. *Acta Geotechnica.* 2016;11(57):177–89.
- [18] Harahap SE, Ou CY. Finite element analysis of time-dependent behavior in deep excavations. *Comput Geotech.* 2020;119:103300.
- [19] Dong YP, Burd HJ, Housby GT. Finite-element analysis of a deep excavation case history. *Géotechnique.* 2016;66(1):1–15.
- [20] Likitlersuang S, Surarak C, Wanatowski D, Oh E, Balasubramaniam A. Finite element analysis of a deep excavation: A case study from the Bangkok MRT. *Soils Found.* 2013;53(5):756–73.
- [21] He X, Xu H, Sabetamal H, Sheng D. Machine learning aided stochastic reliability analysis of spatially variable slopes. *Comput Geotech.* 2020;126:103711.
- [22] Pourtaghi A, Lotfollahi-Yaghin MA. Wavenet ability assessment in comparison to ANN for predicting the maximum surface settlement caused by tunneling. *Tunn Undergr Space Technol.* 2012;28:257–71.
- [23] Zhang W, Zhang R, Wang W, Zhang F, Goh ATC. A multivariate adaptive regression splines model for determining horizontal wall deflection envelope for braced excavations in clays. *Tunn Undergr Space Technol.* 2019;84:461–71.
- [24] Kung GT, Hsiao EC, Schuster M, Juang CH. A neural network approach to estimating deflection of diaphragm walls caused by excavation in clays. *Comput Geotech.* 2007;34(5):385–96.
- [25] Elbaz K, Yan T, Zhou A, Shen SL. Deep learning analysis for energy consumption of shield tunneling machine drive system. *Tunn Undergr Space Technol.* 2022;123:104405.
- [26] Elbaz K, Zhou A, Shen SL. Deep reinforcement learning approach to optimize the driving performance of shield tunnelling machines. *Tunn Undergr Space Technol.* 2023;136:105104.
- [27] Zhang N, Shen SL, Zhou A. A new index for cutter life evaluation and ensemble model for prediction of cutter wear. *Tunn Undergr Space Technol.* 2023;131:104830.
- [28] Chen R, Zhang P, Wu H, Wang Z, Zhong Z. Prediction of shield tunneling-induced ground settlement using machine learning techniques. *Front Struct Civ Eng.* 2019;13(6):1363–78.

- [29] Goh AT, Wong KS, Broms BB. Estimation of lateral wall movements in braced excavations using neural networks. *Can Geotech J.* 1995;32(6):1059–64.
- [30] Zhang R, Wu C, Goh AT, Böhlke T, Zhang W. Estimation of diaphragm wall deflections for deep braced excavation in anisotropic clays using ensemble learning. *Geosci Front.* 2021;12(1):365–73.
- [31] Ma X, Dai Z, He Z, Ma J, Wang Y, Wang Y. Learning traffic as images: a deep convolutional neural network for large-scale transportation network speed prediction. *Sensors.* 2017;17(4):818.
- [32] Zhang WG, Goh ATC, Goh KH, Chew OYS, Zhou D, Zhang R. Performance of braced excavation in residual soil with ground-water drawdown. *Undergr Space.* 2018;3(2):150–65.
- [33] Qu X, Yang J, Chang M. A deep learning model for concrete dam deformation prediction based on RS-LSTM. *J Sens.* 2019;2019:1–4.
- [34] Li J, Li P, Guo D, Li X, Chen Z. Advanced prediction of tunnel boring machine performance based on big data. *Geosci Front.* 2021;12(1):331–8.
- [35] Liu M, Liao S, Yang Y, Men Y, He J, Huang Y. Tunnel boring machine vibration-based deep learning for the ground identification of working faces. *J Rock Mech Geotech Eng.* 2021;13(6):1340–57.
- [36] Kesh tegar B, Nehdi ML, Trung NT, Kolahchi R. Predicting load capacity of shear walls using SVR-RSM model. *Appl Soft Comput.* 2021;112:107739.
- [37] Zhang B, Zhang H, Zhao G, Lian J. Constructing a PM2. 5 concentration prediction model by combining auto-encoder with Bi-LSTM neural networks. *Environ Model Softw.* 2020;124:104600.
- [38] Rao KS, Devi GL, Ramesh N. Air quality prediction in Visakhapatnam with LSTM based recurrent neural networks. *Int J Intell Syst Appl.* 2019;11(2):18–24.
- [39] Zhao R, Yan R, Wang J, Mao K. Learning to monitor machine health with convolutional bi-directional LSTM networks. *Sensors.* 2017;17(2):273.
- [40] Abba SI, Pham QB, Usman AG, Linh NTT, Aliyu DS, Nguyen Q, et al. Emerging evolutionary algorithm integrated with kernel principal component analysis for modeling the performance of a water treatment plant. *J Water Process Eng.* 2020;33:101081.
- [41] vom Scheidt F, Medinová H, Ludwig N, Richter B, Staudt P, Weinhardt C. Data analytics in the electricity sector—a quantitative and qualitative literature review. *Energy AI.* 2020;1:100009.
- [42] Gupta D, Hazarika BB, Berlin M, Sharma UM, Mishra K. Artificial intelligence for suspended sediment load prediction: a review. *Environ Earth Sci.* 2021;80(57):1–39.
- [43] Han Q, Hao Z, Hu T, Chu F. Non-parametric models for joint probabilistic distributions of wind speed and direction data. *Renew Energy.* 2018;126:1032–42.
- [44] Qin B, Xiao F. A non-parametric method to determine basic probability assignment based on kernel density estimation. *IEEE Access.* 2018;6:73509–19.
- [45] D'Agostino RB. Tests for the normal distribution. In *Goodness-of-fit techniques*. England: Routledge; 2017. p. 367–420.
- [46] Calfá BA, Agarwal A, Grossmann IE, Wassick JM. Data-driven multi-stage scenario tree generation via statistical property and distribution matching. *Comput Chem Eng.* 2014;68:7–23.
- [47] Sahu SK, Dey DK, Branco MD. A new class of multivariate skew distributions with applications to Bayesian regression models. *Can J Stat.* 2003;31(2):129–50.
- [48] Brys G, Hubert M, Struyf A. A robust measure of skewness. *J Comput Graph Stat.* 2004;13(4):996–1017.
- [49] Ma K, Chen LP, Fang Q, Hong XF. Machine learning in conventional tunnel deformation in high in situ stress regions. *Symmetry.* 2022;14(3):513.
- [50] Tran TN, Phuc DT. Grid search of multilayer perceptron based on the walk-forward validation methodology. *Int J Electr Comput Eng.* 2021;11(2):1742.
- [51] Zhao Z, Chen W, Wu X, Chen PC, Liu J. LSTM network: a deep learning approach for short-term traffic forecast. *IET Intell Transp Syst.* 2017;11(2):68–75.
- [52] Sherstinsky A. Fundamentals of recurrent neural network (RNN) and long short-term memory (LSTM) network. *Phys D: Nonlinear Phenom.* 2020;404:132306.
- [53] Greff K, Srivastava RK, Koutník J, Steunebrink BR, Schmidhuber J. LSTM: A search space odyssey. *IEEE Trans Neural Netw Learn Syst.* 2016;28(10):2222–32.
- [54] Géron A. Hands-on machine learning with scikit-learn and tensorflow: Concepts, Tools, and Techniques to build intelligent systems. USA: O'Reilly; 2017.
- [55] Huang Z, Xu W, Yu K. Bidirectional LSTM-CRF models for sequence tagging. *arXiv Prepr arXiv:150801991.* 2015.
- [56] Shen SL, Atangana Njock PG, Zhou A, Lyu HM. Dynamic prediction of jet grouted column diameter in soft soil using Bi-LSTM deep learning. *Acta Geotech.* 2021;16(57):303–15.
- [57] Khoshhal J, Mokarram M. Model for prediction of evapotranspiration using MLP neural network. *Int J Environ Sci.* 2012;3(3):1000.
- [58] Ramchoun H, Ghanou Y, Ettaouil M, Janati Idrissi MA. Multilayer perceptron: Architecture optimization and training. *IJIMAI.* 2016;4(1):26–30.
- [59] Ashiquzzaman A, Tushar AK. Handwritten Arabic numeral recognition using deep learning neural networks. In *2017 IEEE International Conference on Imaging, Vision & Pattern Recognition (icIVPR)*. USA: IEEE; 2017, February. p. 1–4.
- [60] Smola AJ, Schölkopf B. A tutorial on support vector regression. *Stat Comput.* 2004;14(3):199–222.
- [61] Zhang H, Cheng X, Li Y, Du X. Prediction of failure modes, strength, and deformation capacity of RC shear walls through machine learning. *J Build Eng.* 2022;50:104145.
- [62] Chen P, Niu A, Liu D, Jiang W, Ma B. Time series forecasting of temperatures using SARIMA: An example from Nanjing. In *IOP Conference Series: Materials Science and Engineering.* Vol. 394. Issue 5. IOP Publishing; 2018, July. p. 052024.
- [63] Ju Y, Sun G, Chen Q, Zhang M, Zhu H, Rehman MU. A model combining convolutional neural network and LightGBM algorithm for ultra-short-term wind power forecasting. *IEEE Access.* 2019;7:28309–18.
- [64] Xia W, Zhu W, Liao B, Chen M, Cai L, Huang L. Novel architecture for long short-term memory used in question classification. *Neurocomputing.* 2018;299:20–31.
- [65] Kardani N, Zhou A, Nazem M, Shen SL. Estimation of bearing capacity of piles in cohesionless soil using optimised machine learning approaches. *Geotech Geol Eng.* 2020;38(2):2271–91.
- [66] Touzani S, Granderson J, Fernandes S. Gradient boosting machine for modeling the energy consumption of commercial buildings. *Energy Build.* 2018;158:1533–43.
- [67] Elnabwy MT, Elbeltagi E, El Banna MM, Elsheikh MY, Motawa I, Hu JW, et al. Conceptual prediction of harbor sedimentation quantities using AI approaches to support integrated coastal structures management. *J Ocean Eng Sci.* 2022. doi: 10.1016/j.joes.2022.06.005.
- [68] Shen SL, Zhang N, Zhou A, Yin ZY. Enhancement of neural networks with an alternative activation function tanhLU. *Expert Syst Appl.* 2022;199:117181.

Appendix

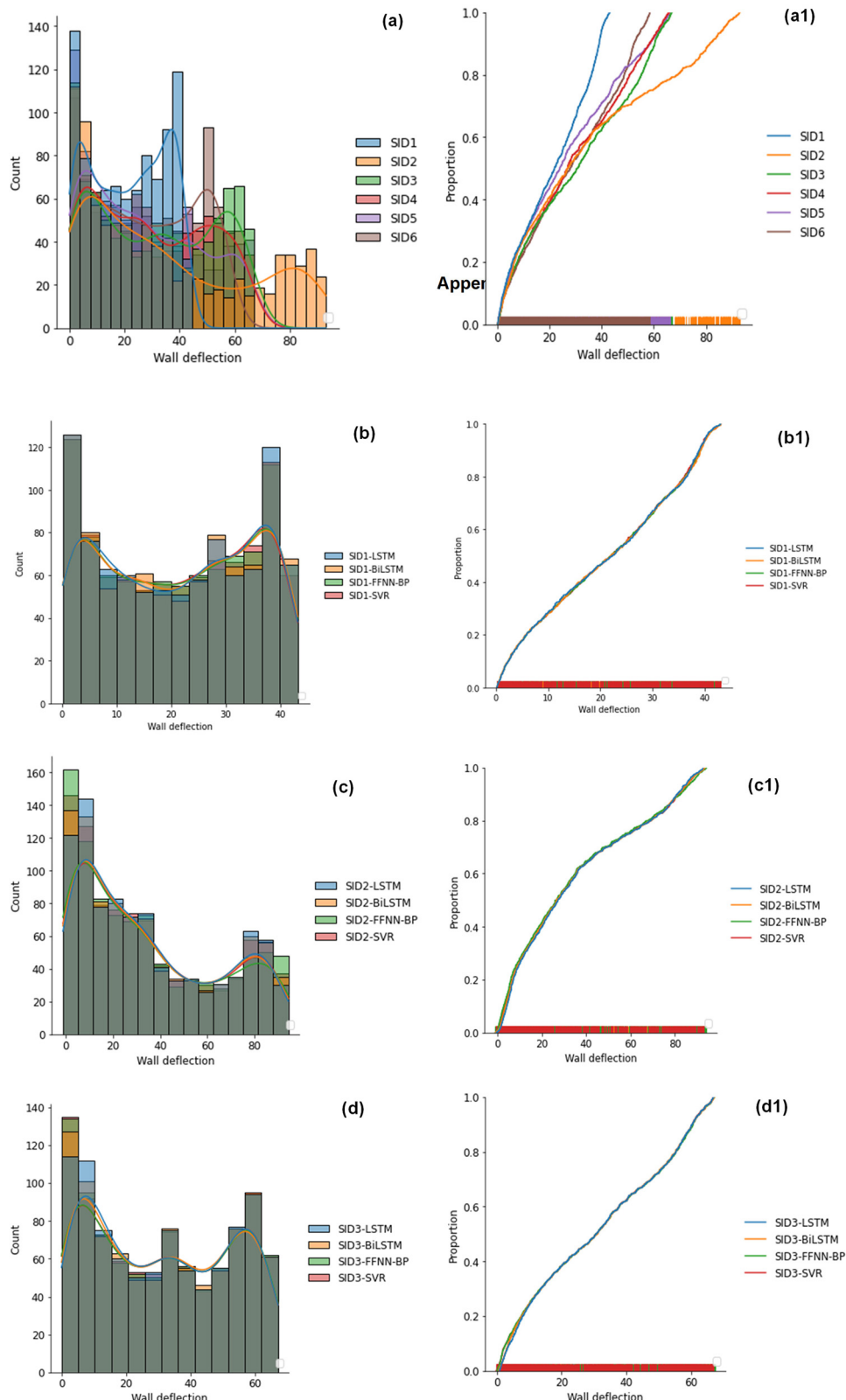
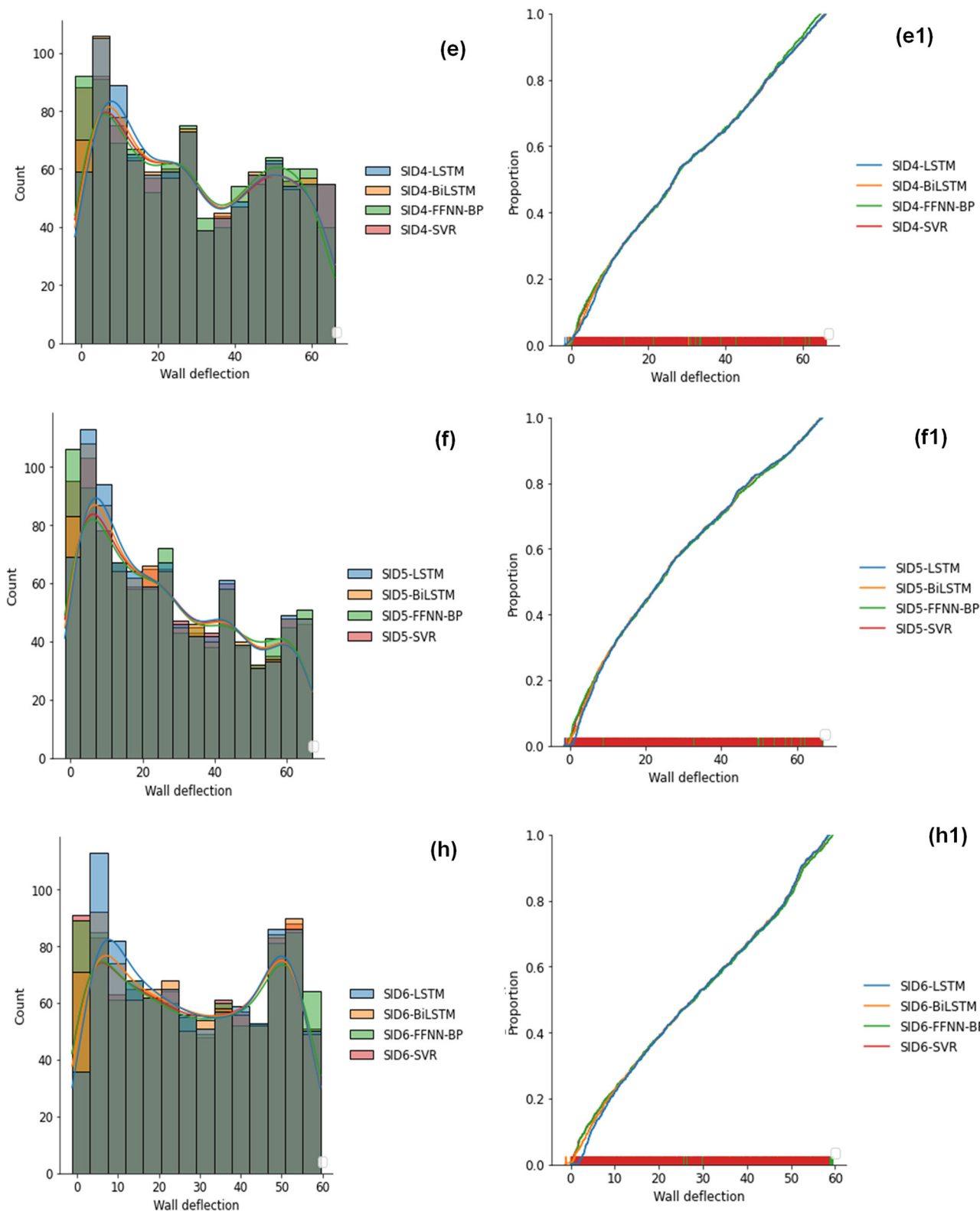


Figure A1: Distribution of input and output variables in the database. Distribution of input variables at SID1, SID2, SID3, SID4, SID5, and SID6 (a, a1). Distribution of output variables at SID1 (b, b1), SID2 (c, c1), SID3 (d, d1), SID4 (e, e1), SID5 (f, f1), and SID6 (h, h1).

**Figure A1:** (Continued)

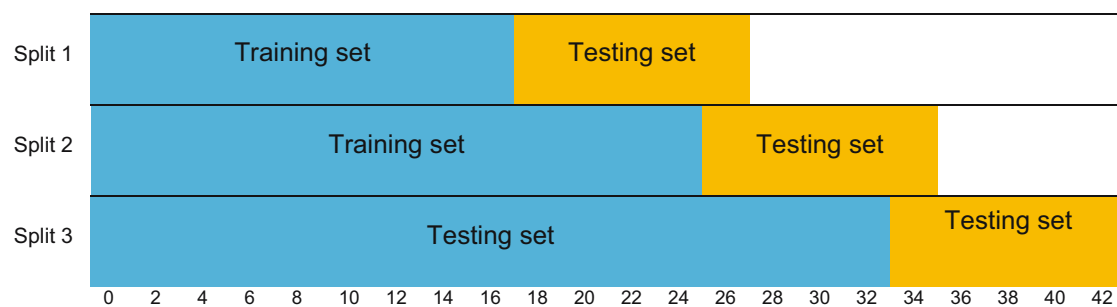


Figure A2: The splitted training and testing data by WVF of input data.